RESEARCH ARTICLE

Robust and Optimized Algorithm for Detection of Copy-Rotate-Move Tempering

ABHISHEK KASHYAP[1], KAPIL DEV TYAGI[1], AND VAIBHAV BHUSHAN TYAGI [ID]2

[1]Department of Electronics and Communication Engineering, Jaypee Institute of Information Technology, Noida 201309, India
[2]Department of Electronics and Communication Engineering, ISBAT University, Kampala, Uganda

Corresponding author: Vaibhav Bhushan Tyagi (tyagi.fict@isbatuniversity.com)

ABSTRACT Since the entire world is covered with computerized digital data, information through digital media is not difficult to move, access, and recycle. Currently, advanced image processing tools are used to create tempered pictures. Using these apparatuses, falsifiers presented forged pictures to spread gossip and rumors. Presently, it is quite difficult for scientific divisions to demonstrate the reality of the original picture. Consequently, a new capable copy-rotate-move tempering recognition algorithm is required. To fulfill this requirement, a computationally efficient technique for copy-rotate-move tempering recognition using Zernike moments and ant colony optimization was proposed. Tests were conducted on various datasets to evaluate the effectiveness of the proposed method. The results were compared with those of the previously proposed state-of-the-art method, using metrics such as F1 score, recall, and precision. It is evident that the proposed method outperforms the currently used state-of-the-art methods.

INDEX TERMS Ant colony optimization, copy-move, frequency domain, forgery localization, image processing, image forensics, principal component analysis, wavelet decomposition, Zernike moment invariants, rotation-invariant.

I. INTRODUCTION

In general, digital pictures are a basic part of everyone is life and are extensively utilized as a mode of correspondence, protection handling, observation frameworks, intelligence services, criminological examinations, political fights, and clinical imaging [1], [2], [3], [4]. Cloning is the most well-known picture control method, in which a part of a picture is copied and pasted into a similar picture to create a spliced picture that is forged, making it difficult to recognize cloning with our unaided eyes [5], [6], [7]. Various experts have proposed a variety of copy-move temper detection strategies. In [8] the authors proposed a strategy based on an obscure second invariant for copy-move tamper detection. This depends on the block-based strategy. Fridrich et al. [9] suggested a way to see the changed part, at least when the copied area is upgraded, changed, or joined with the base and when the changed image is saved in the JPEG format. The method proposed in [10] uses principal component analysis (PCA) on tiny fixed-size image blocks to generate a lower

estimation depiction that is sensitive to small differences in the image. However, this results in a lossy compression or additive noise. In [11], the authors suggested a calculation to distinguish copy-rotate-move fraud, which depends on singular value decomposition, and separated highlight vectors, which have some essential characteristics of mathematical invariance and harshness to commotion. Bayram et al. [12] introduced a strategy for perceiving copy-move imitation in computerized pictures that is amazingly more vivacious for lossy compression, revolution, and scaling types of controls. Using radix sort, Lin et al. [13] suggested a powerful methodology for copy-move falsification recognition that can fend against various attacks, such as Gaussian commotion and JPEG compression. Huang et al. [14] demonstrated a system based on an improved discrete cosine transform (DCT) to detect duplicate move fraud in any case when a picture was distorted by obscuring, JPEG compression, or an additional substance such as white Gaussian noise. In light of the discrete wavelet transform (DWT), Zhang et al. [15] developed a novel blind criminology calculation for recognizing copy-move imitation, which is robust to various types of copy-rotate-move temper recognition with lower

The associate editor coordinating the review of this manuscript and approving it for publication was Gerard-Andre Capolino.

computational complexity. In [31], the authors suggested a strategy for copy-rotate-move temper recognition based on wavelet decay, and investigated the reduction in handling time using wavelet decomposition; regardless of how the improvement is important, the results are still far from good in situations where they can be measured, and [28] suggests a technique to further develop copy-move temper recognition with the assistance of particle swarm optimization (PSO). Researchers have also estimated optimized parameters using PSO [37], [38]. In [37], a novel approach for locally adaptive filtering was suggested based on the RBF kernel smoother with a variable width. The asymmetrical combined-window relative intersection of confidence intervals (RICI) approach, the parameters of which are optimized using a PSO-based method. The details of the PSO method for parameter estimation are given in [38]. The authors proposed a calculation in [42] to recognise copy-move imitation using wavelet decomposition and firefly optimization. In terms of the discovery rate, this strategy outperforms most existing techniques, particularly block-based ones. In [46], the authors proposed a calculation based on a complex wavelet transform that uses local binary patterns and is equipped to identify erratic levels of the pivot, unlike existing procedures, which are utilized to enhance misleading matches due to normally comparable blocks in a picture. The introduced approach is an invariant to pivot, which is essentially attributable to the use of visual descriptors to address pictures using the proposed method. In [51], the authors suggested copy-move phony identification, which includes five phases: initialization of the image, division of the image into covering blocks, computation of the standard deviation and mean of each block, highlight parameters, and lexical arrangement. The support vector machine (SVM) classifier was then used to determine whether the image was genuine or manipulated.

In [56], the authors suggested a method for detecting copy-move forgery, that combines binary robust invariant scalable keypoints (BRISK) and speeded-up robust features (SURF) descriptors. The SURF characteristics scan can withstand a variety of post-processing assaults, including rotation, blurring, and added noise. Although scale-invariant forged areas and poorly localised keypoints of objects inside the forged picture are difficult to discern, the BRISK characteristics are thought to be reliable in this regard.

In [57], the authors suggested a copy-move forgery detection method, in which the contrast of the input image is modified using the dynamic histogram equalisation (DHE) approach. The features of the manipulated images are extracted using an SURF descriptor, which is then matched using the Euclidean distance. The matched characteristics are subjected to unique binary mask generation and copy-move forgery area detection method known as modified density-based spatial clustering of applications with noise (mDBSCAN).

In [58], the authors suggested a calculation to identify copy-move phony identification, which was fragmented into two subpictures using quadtree decomposition to achieve this objective. The sub-pictures were marked as smooth and complete. The local binary pattern rotation invariant (LBPROT) approach was used to obtain the textural structure of the smooth marked portion. The key points were then separated from the finished portion and the textural type of the smooth portion. From this point forward, they coordinate with each other to acquire falsified pieces of information. By coordinating the separated keypoints, researchers determined whether a picture was manufactured. The authors proposed a dense invariant representation (DIR) in [59], which is a new framework for representing forensics characterised by stable descriptions and mathematical guarantees. The primary objective of this study was to offer a systematic approach to image representation in forensic activities.

In [61], the authors offered two sequentially built subnetworks, the copy-move similarity detection network, and the source/target area distinguished network to ensure identification of the source and target regions. In [63], [64], and [65], the authors suggest orthogonal moments that can be used for feature extraction such as discrete Hahn polynomials (DHPs) and their moments are considered to be one of the most efficient orthogonal moments.

In conclusion, researchers have proposed a variety of techniques to address the issue of copy-move tampering in digital images. These techniques include block-based strategies, obscure second invariants, principal component analysis (PCA), singular value decomposition (SVD), radix sort, discrete cosine transform (DCT), discrete wavelet transform (DWT), particle swarm optimization (PSO), wavelet decomposition, firefly optimization, complex wavelet transform, binary robust invariant scalable keypoints (BRISK), speeded-up robust features (SURF), dynamic histogram equalization (DHE), modified density-based spatial clustering of application with noise (mDBSCAN), quadtree decomposition, local binary pattern rotation invariant (LBPROT), dense invariant representation (DIR), and orthogonal moments. Although existing methods have shown promising results, they still have limitations in terms of computational costs, robustness against geometric transformations, and resistance to other image alterations. Also, due to the large number of features and lack of robustness against geometric transformation attacks, most block-based algorithms have significant computational costs and are not resistant to other alterations such as JPEG compression, scaling, noise addition, and rotation.

In this study, we proposed a novel copy-rotate-move temper recognition method (CRMFD-ACO) that combines wavelet decomposition, Zernike moments, and ant colony optimization. Our experimental results demonstrated the superiority of the proposed method in terms of precision, recall, and F1-score compared with existing methods, particularly block-based methods. Based on experimental findings from publicly accessible datasets, the proposed approach outperforms state-of-the-art techniques, including conventional algorithms and deep learning-based networks. Our results
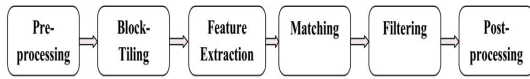
FIGURE 1. Flowchart of a block-based copy-rotate-move tempering recognition framework.

demonstrated that the proposed strategy is robust under JPEG compression, scaling, noise addition, and rotation assaults. Overall, our work contributes to the advancement of copy-move temper detection techniques by providing a robust and efficient approach for detecting manipulated regions in digital images.

Rest of the paper is organized as follows: In Part I, fake photo recognition is presented. The problem is described in Section II. In Section III, we outline our approach to copy-rotate-move region recognition using an ant colony optimization algorithm and Zernike moment invariants. The findings on computer recreation are presented in Section IV. Conclusions and scope for future research are presented in Section V.

II. PROBLEM FORMULATION

In general, copy-rotate-move temper identification procedures use supporting innovations, such as pre-handling, sliding the block, extracting the feature, filtering, matching similar blocks, and handling. This is primarily a block-based structure, as shown in Fig. 1. The results of tests against various imitation pictures or lessons learned from prior experience limit these optimized values because the optimum values of the chosen parameters also affect the simulation results. However, unmistakable detection chooses a variety of distinct values and, appropriate for explicit images. When used to examine a wide range of created images, the following imperatives are present: matching block pairs cannot identify the fashion area when matching conditions are satisfied. When there is an excessive number of comparison blocks in the provided picture and the boundary values are chosen incorrectly, the fashion area is not replicated. In any case, a few comparative regions are perceived, which are misidentified as fashioned regions. In any case, these regions are in the vicinity of the original image.

III. PROPOSED APPROACH

When it comes to ant colony optimization, the goal of the proposed method is to find plausible optimum parameter values for each evaluated picture that make sense intuitively. Fig. 2 shows the exhaustive CRMFD-ACO flow diagram. The first stage of this technique involved elemental or basic detection. The second stage is parameter assessment. The block-based construction and parameter evaluation used in the copy-rotate-move phony detection activity, which is part of the natural recognition element, are used to provide realistic boundary values that aid in characterizing duplicated areas. To the best of our knowledge, this strategy has not yet been used by scientists. With the help of suitable
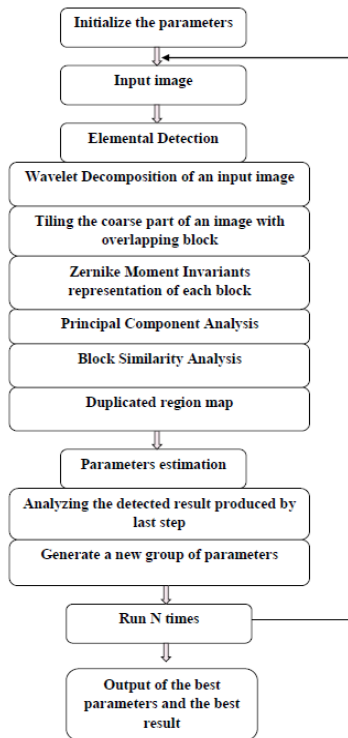
border values, the managed image may provide favorable outcomes. Appropriate boundary values were evaluated using ant colony optimization (ACO) [16]. To the best of our knowledge, no copy-rotate-move tempering identification approach currently employs the ACO. The goal of the proposed algorithm is to understand the input data and output value, which includes a picture, where the output value is the number of matched blocks and group of borders. This value is used to determine the performance of the algorithm. The best-matched building blocks were used to construct an assessment model that was used to acquire an improved outcome. In addition, the optimal arrangement appears when such an assessment standard includes a high value.

A. ANT COLONY OPTIMIZATION

Researchers have developed a number of "strong" or "powerful" ant colony algorithms in light of these ant behavior characteristics, and substantial progress has recently been achieved in this area. Marco Dorigo led research in this area in 1992 [16], [17]. Several variants have been identified to date. If we use some of the characteristics of ant behavior and add new ones, we can create a new class of computation and algorithms. The possibility of choosing a route and pheromone disappearance rate are two important factors in this situation. Although this is still an active area of research, there are only a few methods to address these problems. In this section, we outline the current winning tactics. The probability that ants at a certain hub r will choose the path from hub r to hub s is given by [16]:

$$q_{rs} = \frac{\psi_{rs}^{\gamma} a_{rs}^{\delta}}{\sum_{r,s=1}^{m} \psi_{rs}^{\gamma} a_{rs}^{\delta}} \qquad (1)$$

where $\gamma > 0$ and $\delta > 0$ are the impact boundaries and their generally used qualities are $\gamma \approx \delta \approx 2$. Pheromone fixation on the path between r and s is known as ψ_{rs}, and the attractiveness of a comparable route is known as a_{rs}. Nearly prior course or route information, such as distance b_{rs}, is frequently used for $a_{rs} \propto 1/b_{rs}$, implying that more constrained courses will be chosen because of their shorter travel time; as a result, the pheromone focusing on these courses is higher. When the voyaging time was shorter, fewer pheromones were lost. The probability formula closely resembles how ants generally choose to move in directions with higher pheromone concentration [18]. The chance of an ant choosing a path is correlates with pheromone fixation on the path in the simpler scenario when $\gamma = \delta = 1$. The chance is normalized by the denominator, making it within the range of zero to one. The evaporation or disappearance of pheromones causes their concentrations to fluctuate over time. Additionally, the upside of pheromone dissipation allows the framework to attempt to avoid being trapped in the neighboring optima. If there is no dissipation, the method in which the initial ants randomly choose will eventually becomes the preferred method because of the attraction that their pheromone causes to other ants, as shown in Fig. 3. For a constant rate of pheromone rot or dissipation, pheromone fixation usually varies exponentially

FIGURE 3. Basic concept of ant colony optimization (i) initial ant behaviour and (ii) ant behaviour after some time to achieve the optimum path or solution in the ant colony optimization algorithm.

FIGURE 2. Flowchart for the proposed approach to detect copy-rotate-move forgeries based on Zernike moment invariants and ant colony optimization.
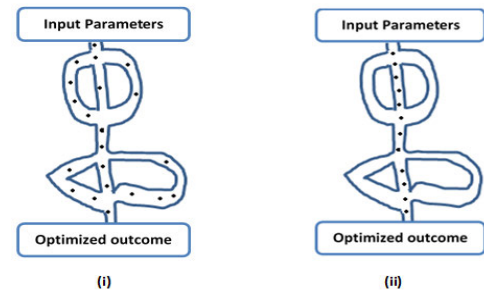
with time [18]:

$$\psi(t) = \psi_0 e^{-\alpha t} \tag{2}$$

where t is time and ψ_0 is the underlying pheromone central-ization. If $\alpha t \ll 1$, then $\psi(t) \approx (1 - \alpha t)\psi_0$ at that point. Vanishing can be calculated as $\psi^{t+1} \leftarrow (1 - \alpha)\psi^t$ for the unitary time increase $\triangle t = 1$. Consequently, the updated pheromone formula is [18]:

$$\psi_{rs}^{t+1} = (1 - \alpha)\psi_{rs}^t + \beta\psi_{rs}^t, \tag{3}$$

where $\alpha \in [0, 1]$ is the rate at which the pheromone dis-appears. The amount of pheromone preserved at the time t along path r to s when an ant travels a distance D is known as the augmentation $\beta\psi_{rs}^t$. Normally $\beta\psi_{rs}^t \propto 1/D$. If there are no ants on a route, then there is no stored pheromone.

There were several minor deviations from this method. Utilizing certain pheromone concentration restrictions and allowing only the ants with the most advanced global solution(s) to store pheromones is a possible strategy for increasing speed. It is also possible to use design wellness placement. The crucial ACO processes is discussed from the pseudo-code, as shown in Algorithm 1. However, there are still more studies that may be more dynamic. Because a complex network structure is always composed of distinct hubs, this method can be used to intelligently and effectively address complicated routing problems. Fig. 4 shows a flow

chart for the parameter estimation of the proposed algorithm using ant colony optimization.

B. ELEMENTAL DETECTION

Six stages comprise the proposed elemental detection for copy-rotate-move imitation recognition. This includes wavelet decomposition of the test image, sliding coarse parts of the image with superimposed grids or blocks, an invariant representation of each sliding block using Zernike moments, PCA for dimensional reduction, an examination of the block's similarity or likeness, and a tempered region map as the sixth and final stages of smart image imitation recognition. To strengthen the portrayal, start with a picture of size $(X \times Y)$ pixels.

1) WAVELET DECOMPOSITION

When a test image is processed through wavelet decomposi-tion, four nuances of the test image are obtained: diagonal, vertical, horizontal, and detail of the coarse area of the test image. The scaling function $\kappa(w)$ and Harr Wavelet $\varphi(w)$ are orthogonal to each other, according to [53], [54], and [55].

$$\varphi(w) = \sum_{n=-\infty}^{\infty} (-1)^n k_{Y-1-n}\sqrt{2}\kappa(2w - n) \tag{4}$$

Description of wavelet decomposition of the two-dimensional image function $f(c, d)$ is given below [55]:

$$f(c, d) = \sum_{u=-\infty}^{\infty} \sum_{o=-\infty}^{\infty} \sum_{p=-\infty}^{\infty} g_{u,o,p}\varphi_{u,o}(c)\varphi_{u,p}(d) \tag{5}$$

2) SLIDING THE IMAGE WITH A SUPERIMPOSED GRID

Coarse portion of the test image was used for fur-ther analysis after the wavelet decomposition. A pixel-by-pixel superimposed grid of size $(Z \times Z)$ is pushed over the handled picture from top to bottom and left to right. Therefore, the total number of covering blocks is $(X - Z + 1) \times (Y - Z + 1)$ when an image of size $(X \times Y)$ is processed. One presumption, in this case, is that the dupli-cated region is larger than the superimposed grid or block size.

Algorithm 1 Pseudo Code of the Ant Colony Optimization Algorithm

1: *Start*
2: Instate
3: **while** Stopping criterion not fulfilled **do** Position every ant in a beginning hub
4:     **repeat**
5:         **for** every ant **do** Choose next hub by applying the state transition rule. Apply step by step pheromone update
6:         **end for**
7:     **until** each ant has fabricated an answer or solution
8:     Update best arrangement or solution
9:     Apply offline pheromone update
10: **end while**
11: *End*

Algorithm 2 Pseudo Code of the Proposed Algorithm for Copy-Rotate-Move Forgery Detection

1: *Start*
2: Initialize the parameters
3: **while** Stopping criterion not fulfilled (Maximum value of G match) **do** Perform elemental detection for each text image.
4: (i) Wavelet decomposition of the text image
5: (ii) Tiling the coarse part of the image with overlapping block
6: (iii) Zernike moment invariants representation of each block
7: (iv) Principal component analysis
8: (v) Duplicated region map
9:     **repeat**
10:         **for** each stage **do** Choose a new group of parameters in parameters optimization using Ant Colony Optimization. Perform elemental detection for each group of parameters
11:         **end for**
12:     **until** each stage has fabricated an answer or solution
13:     Update best arrangement or solution
14: **end while**
15: *End*

---

3) SUPERIMPOSING BLOCK'S REPRESENTATION BY THE ZERNIKE MOMENT INVARIANTS

Zernike moments were determined for each overlapping block. The moment invariant function is widely utilized for feature extraction in pattern recognition, digital watermarking, and other important applications [19], [20]. Moment invariants of the processed picture have better characteristics against rotation and thus play an important role in recognizing copy-rotate-move phony. Because they are less susceptible to image noise, easier to compute higher-order moments, and better able to express structural attributes [20], [21], [22],
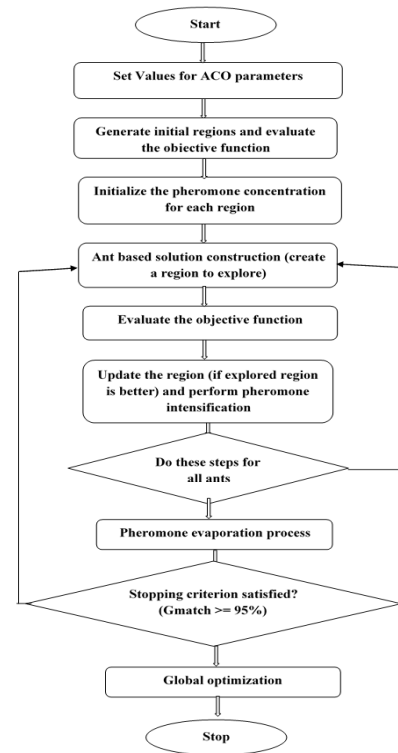
FIGURE 4. Flowchart for parameter estimation of the proposed approach through ant colony optimization.

Zernike moments are superior to other moment algorithms currently in use. The Zernike moments of the continuous image function $f(c, d)$ [23] are expressed as:

$$A_{xz} = \frac{x+1}{\pi} \int \int_{c^2+d^2 \leq 1} f(c, d) V_{xz}^*(\rho, \theta) d(c) d(d), \quad (6)$$

where b is the order and non-negative integer, and c is the repetition and integer such that $(x - |z|)$ is also even and non-negative. The complex-valued function $V_{xz}(c, d)$ is characterized as [23]:

$$V_{xz}(c, d) = V_{xz}(\rho, \theta) = R_{xz}(\rho) exp(jz\theta), \quad (7)$$

where ρ and θ are the polar coordinates over the unit circle, and R_{xz} is the Zernike polynomial or polynomial of ρ, which is denoted as follows [23]:

$$R_{xz}(\rho) = \sum_{v=0}^{(x-|z|)/2} \frac{(-1)^v [(x - v)!] \rho^{x-2v}}{v!(\frac{x+|z|}{2} - v)!(\frac{x-|z|}{2} - v)!}. \quad (8)$$

This polynomial is satisfies the orthogonality property, which is defined as [23]:

$$\int \int_{c^2+d^2 \leq 1} [V_{xz}^*(c, d)] \times V_{ef}(c, d) d(c) d(d) = \frac{\pi}{x+1} \delta_{xe} \delta_{zf},$$

$$where \; \delta_{ij} = \begin{cases} 1, & i = j \\ 0, & otherwise. \end{cases} \quad (9)$$

These integrals are replaced by the summations for the digital picture, the center of the block is the starting point for the

computation of Zernike moments, and the pixel coordinates are mapped with the unit circle. These pels were not utilized for the computation of the Zernike moments outside the unit circle. Consider ϑ is the rotation angle and the rotated picture is defined in terms of f_r, then the relationship between the rotated and original picture is represented as [23]:

$$f_r(\rho, \theta) = f(\rho, \theta - \vartheta). \tag{10}$$

By using eq. 6 and 7, A_{bc} can be written as:

$$A_{xz} = \frac{x+1}{\pi} \int_0^{2\pi} \int_0^1 f(\rho, \theta) V_{xz}^*(\rho, \theta) \rho d\rho d\theta$$
$$= \frac{x+1}{\pi} \int_0^{2\pi} \int_0^1 f(\rho, \theta) R_{xz}(\rho) exp(-jz\theta) \rho d\rho d\theta. \tag{11}$$

Consequently, the following equations can be used to express the Zernike moments for the rotated image at the same coordinate [23]:

$$A'_{xz} = \frac{x+1}{\pi} \int_0^{2\pi} \int_0^1 f(\rho, \theta - \vartheta) R_{xz}(\rho) exp(-jz\theta) \rho d\rho d\theta. \tag{12}$$

From the change in variable $\theta_1 = \theta - \vartheta$, Eq. 12 can be written as [23]:

$$A'_{xz} = \frac{x+1}{\pi} \int_0^{2\pi} \int_0^1 f(\rho, \theta_1) R_{xz}(\rho) \qquad exp(-jz(\theta_1 + \alpha))$$
$$\times \rho d\rho d\theta_1 \tag{13}$$

$$A'_{xz} = \left[\frac{x+1}{\pi} \int_0^{2\pi} \int_0^1 f(\rho, \theta_1) R_{xz}(\rho) \quad exp(-jz\theta_1) \rho d\rho d\theta_1 \right]$$
$$\times exp(-jz\vartheta) \tag{14}$$

$$A'_{xz} = A_{xz} exp(-jz\vartheta). \tag{15}$$

Each Zernike moment exhibited a phase shift during rotation, as shown in Eq. 15. $|A_{xz}|$ is defined as the magnitude of the Zernike moments, which is used as an invariant feature against rotation for the processed picture. Therefore, the computation of the magnitude part of the Zernike moments plays an important role in determining copy-rotate-move phony.

4) PCA-BASED DIMENSIONAL REDUCTION
Using the Zernike moment invariants of each sliding grid, we can reduce the dimensions of the feature vector in this stage. It comprises all the important information from the coarse portion of the image created by wavelet decomposition. For a basic grasp, the following is a review of the fundamentals of PCA [4]:

$$\overrightarrow{\mathbf{H}} = (h_1, h_2, h_3, h_4, \dots h_{e0}, \dots h_e). \tag{16}$$

We should only consider the e_0 terms from the e terms and ignore the $(e - e_0)$ terms to reduce the component of the feature vector $\overrightarrow{\mathbf{H}}$, its lower bound is 8 and the upper bound is 24, as shown in Table 1. The e_0 value was optimized

using the ant colony optimization algorithm. The transform matrix T is used to change the vector of dimension e from one space to another, because no one knows where the most extreme data or information in the supplied feature vector is located. This phenomenon can be used to generate a new feature vector $\overrightarrow{\mathbf{H}}_{new}$ with extremely high-variance feature values.

$$T\overrightarrow{\mathbf{H}} = \overrightarrow{\mathbf{H}}_{new} \tag{17}$$

$$U_i = \overrightarrow{\mathbf{H}}^T \overrightarrow{\mathbf{V_i}} = \overrightarrow{\mathbf{V_i}}^{\mathbf{T}} \overrightarrow{\mathbf{H}} \tag{18}$$

$$\overrightarrow{\mathbf{H}} = \sum_{i=1}^{m} U_i \overrightarrow{\mathbf{V_i}} \tag{19}$$

$$E[U_i U_j] = \lambda_i \delta_{ij}; \quad if \Rightarrow i = j \ \epsilon \ 1; i \neq j \ \epsilon \ 0; \tag{20}$$

$$E[\overrightarrow{\mathbf{V_i}}^{\mathbf{T}} \overrightarrow{\mathbf{H}} \overrightarrow{\mathbf{H}}^T \overrightarrow{\mathbf{V_j}}] = \lambda_i \delta_{ij} \tag{21}$$

$$\overrightarrow{\mathbf{V_i}}^{\mathbf{T}} E[\overrightarrow{\mathbf{H}} \overrightarrow{\mathbf{H}}^T] \overrightarrow{\mathbf{V_j}} = \lambda_i \delta_{ij} \tag{22}$$

$$\overrightarrow{\mathbf{V_i}}^{\mathbf{T}} \overrightarrow{\mathbf{R}} \overrightarrow{\mathbf{V_j}} = \lambda_i \delta_{ij} \tag{23}$$

$$\overrightarrow{\mathbf{R}} \overrightarrow{\mathbf{V_i}} = \lambda_i \overrightarrow{\mathbf{V_i}} \tag{24}$$

where U_i is the projection, and $\mathbf{V_i}$ is the orthogonal basis. On the off chance that the condition addressed in equation (23) is satisfied then the condition displayed in equation (24) is satisfied. Once the eigenvalues are arranged in a decreasing order, the slashing action starts.

5) BLOCKS SIMILITUDE EXAMINATIONS
Euclidean distance was used to determine the proximity of the sub-blocks. Assuming that they have a smaller Euclidean distance, these sub-blocks seem to be comparable. Even if this is a crucial situation, it is not the only parameter for detecting tempering. In addition, the sub-block circumstances and nearby neighborhoods were examined to obtain an accurate replica. If the neighborhoods of these sub-blocks are also equivalent and the distances between them should not be exactly R, then there is a high probability that these blocks will be mimicked and designated as imitation regions. The use Euclidean distance symbol ρ allows the resemblance measure $B(S_c, S_d)$ [8] between two sub-blocks c and d to be detected. Sub-blocks c and d have values of $1, 2, \dots (X - Z + 1) \times (Y - Z + 1)$ and are addressed as follows:

$$B(S_c, S_d) = \frac{1}{1 + \rho(S_c, S_d)} \tag{25}$$

$$\rho(S_c, S_d) = \left(\sum_{f=1}^{Y} (S_c[f] - S_d[f])^2 \right)^{1/2} \tag{26}$$

If $B(S_c, S_d) \geq T$, an additional investigation has already been conducted for the adjacent blocks S_c and S_d. The threshold (T) assumes an extremely important role in determining the level of dependability among sub-blocks c and d; this will lay out the bare minimum criteria for selecting tempered
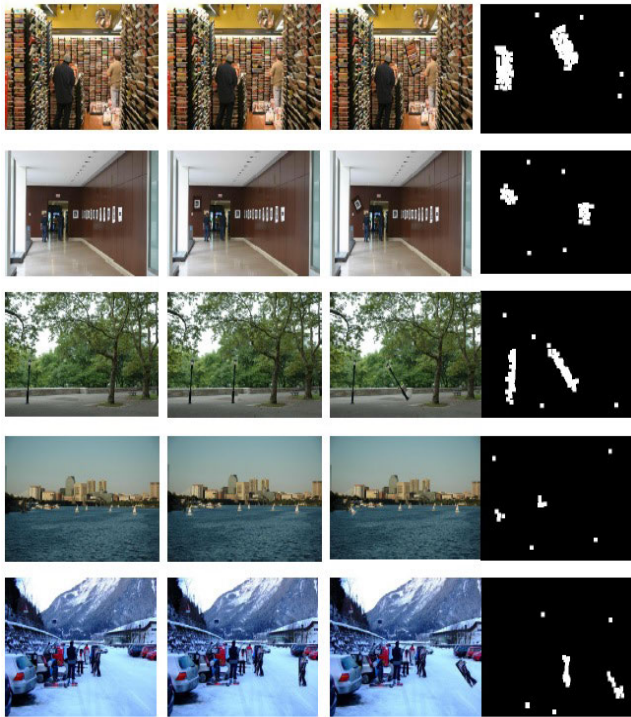
FIGURE 5. Some examples of genuine pictures are included in the first column, followed by their altered pictures in the second column, and the corresponding recognition results are reported in the third column based on DB-1.
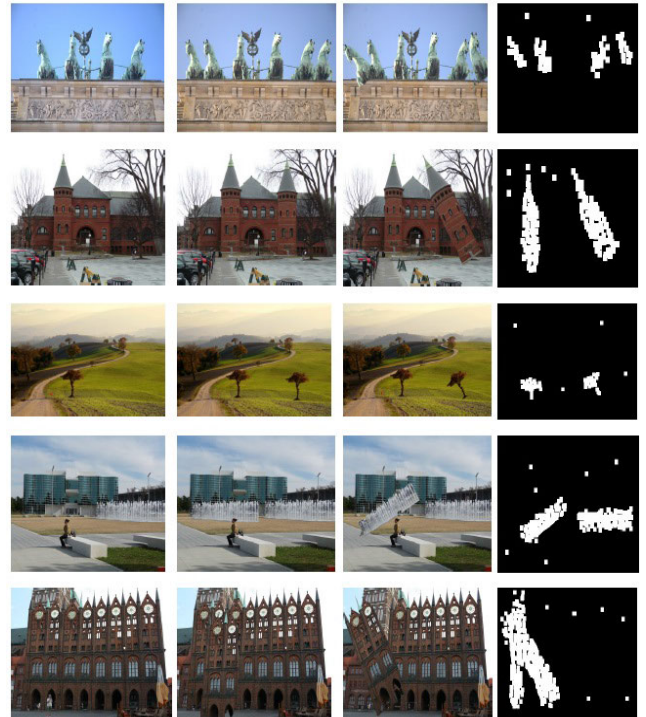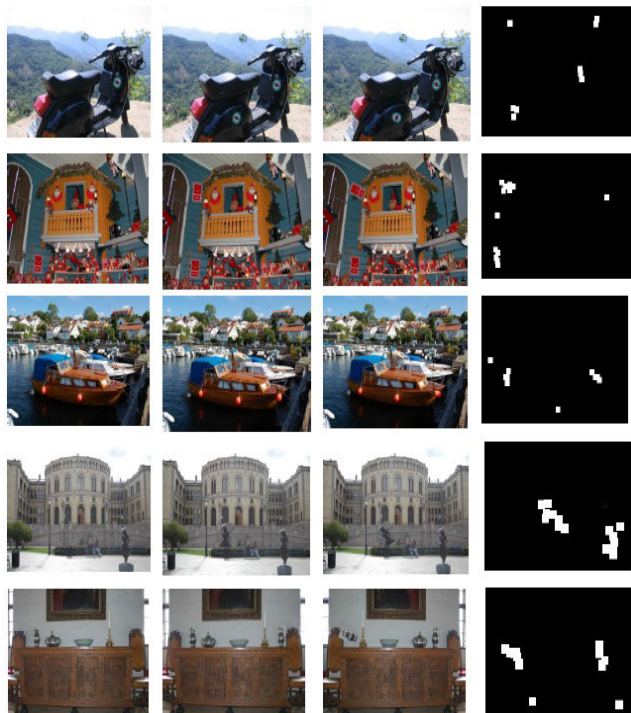

FIGURE 6. Some examples of genuine pictures are included in the first column, followed by their altered pictures in the second column, and the corresponding recognition results are reported in the third column based on DB-2.

regions. Sixteen adjacent sub-blocks, such as 4 sub-blocks at the bottom, four at the top, four at the right, and four at the left, were taken from the dissected sub-block for neighborhood operation.

$$B\left(block\left(c + u_v, d + v_v\right), block\left(e + u_v, f + v_v\right)\right) \geq T \tag{27}$$

where $v \in (-4, -3 \ldots 4)$ and r (no. of neighbourhoods) = $1 \ldots 16$.

If $B(block(c, d), block(e, f)) \geq$ T, but

$$\sqrt{\left((c - e)^2 + (d - f)^2\right)} \leq R \tag{28}$$

Precise tempered region in the tempered image was obtained using conditions (27) and (28). When the equivalence measure between the sub-blocks is more evident than the threshold value T, the separation between these sub-blocks should not be exactly equal to R. This is a crucial need for further research on proximity measures between sub-blocks for forgery recognition. The minimum distance between the tempered regions was represented by the parameter value R. With the help of these conditions, more exact temperate areas were obtained. Finally, a matrix Q of the same size as that of coarse section of the image was obtained. If the sub-block at that point is tempered, the pixels of this matrix are set to one; otherwise, they are set to zero.

6) TEMPERED REGION MAP

Acquisition of a tempered region map involves the addition of each component of $I(c, d)$ to its specific component of $Q(c, d)$.

C. ASSESSMENT CAPABILITY FOR PARAMETER ENHANCEMENT OR OPTIMIZATION

Approximate solution to challenging optimization issues can be found using a population-based metaheuristic known as ant colony optimization (ACO). In ACO, a group of software agents, referred to as artificial ants, look for good solutions to a specific optimization issue. It is modeled after how ants forage for food. Initially, the ants were scurry about aimlessly. As an ant locates a food source, it leaves "markers" (pheromones) on the trail leading back to the colony to indicate the location of the food source. ACO employs the alpha, beta, and evaporation rate factors to determine the optimal solution on a probabilistic basis. In the proposed algorithm, a block-based structure was used to present the enhancement parameters listed in table 1. Condition 29 describes the assessment capability, which is the objective function of the proposed algorithm. Our aim was to optimize this objective function to determine the optimal solution using ACO. The blocks with distances that are not exactly R and that do not participate in the evaluation criterion are referred to as true matched blocks TMB_t and mismatched blocked MMB_t, respectively. The mismatch coefficient ϕ

TABLE 1. Lower and upper bounds of optimized parameters used in proposed approach for copy-rotate-move forgery detection.

Parameters	Meaning	Lower bound	Upper bound
Z	Scale of the grid	4	36
r	The number of neighborhoods	4	24
R	The shortest distance between each block	8	50
T	Threshold	.001	.95
e_0	The number of feature vectors	8	24

FIGURE 7. Some examples of genuine pictures are included in the first column, followed by their altered pictures in the second column, and the corresponding recognition results are reported in the third column based on DB-3.

provides the least default incentive for the faulty blocks. The chance of an actual match is denoted by the variable G_{match}, which is used to estimate the tempered region in a fashioned image. The stopping criterion for forged region detection is satisfied when the maximum value of G_{match}, is greater than or equal to 95% of the matched block for forged region detection, indicating that an optimal solution has been obtained.

$$G_{match} = \frac{TMB_t}{TMB_t + \phi}, \phi = \begin{cases} MMB_t, & MMB_t > R \\ 10, & MMB_t \leq R \end{cases} \quad (29)$$

IV. EXPERIMENTS AND RESULTS

A. MEASUREMENTS

Key metrics are *precision(p)*, *recall(r)*, and F_1-score, which depend on whether a result is evidently positive or truly positive, falsely positive or misleadingly positive, or falsely negative, as shown in conditions 30 and 31, [66] respectively.

$$p = \frac{T_P}{T_P + F_P}, and \quad r = \frac{T_P}{T_P + F_N}. \quad (30)$$

$$F_1 = 2.\frac{Precision.Recall}{Precision + Recall} = \frac{2T_P}{2T_P + F_N + F_P}. \quad (31)$$

B. RESULTS

This section presents the results of the proposed algorithm after testing on the datasets MICC-F220 (DB-1) [62], MICC-F600 (DB-2) [62], and MICC-F2000 (DB-3) [62]. To compare the proposed method to existing techniques such as Babak [8], Fridrich et al. [9], Popescu and Farid [10], Kang et al. [11], Bayram et al. [12], Lin et al. [13], Huang et al. [14], Zhang et al. [15], Wavelet Dec. [31], PSO [28], CMFD-FA [42], Dixit and Nascar [46], Ahmed at al. [51], DBSCAN [56], DHE-SURF [57], Quadtree [58], Qi et al. [59], and Chen et al. [61], several performance indicators including F1-score, recall, and precision are computed. The proposed method was implemented using MATLAB R2021a and a 3.98 GHz Intel(R) Core(TM) i7-9750H CPU with 16 GB RAM and GTX1050. A total of 220 images of MICC-F220 (DB-1) were divided into 110 altered and 110 unaltered images. For DB-1, a few real and tempered pictures and their detection outcomes are shown in Fig. 5. Tests were conducted to calculate the parameters specified by conditions 30 and 31. Table 2 lists the F1-score, recall, and precision for the proposed and specific existing systems based on DB-1. The proposed technique had an average F1-score, recall, and precision of 93.15%, 91.89%, and 94.44%, respectively. The estimated accuracy for recognizing ill-defined situations in doctored images was 3.41%. This was obtained after a blind experiment was conducted by using a mixture of tempered and real images from the dataset. Compared with the current methods, it was determined that the proposed algorithm achieved higher improvements in the F1-score, recall, and precision from 1.16% to 8.41%, 1.01% to 7.62%, and 0.55% to 8.27%, respectively.

MICC-F600 (DB-2) dataset consisted of 440 real images, 160 tempered images, and 160 ground-truth images. In light of DB-2, a few real pictures, tempered pictures, and their detection outcomes are shown in Fig. 6. As shown in Table 3, the average F1-score, recall, and precision of the proposed technique were 93.68%, 92.09%, and 95.32%, respectively, and the accuracy of the estimated recognition of ill-defined situations of doctored pictures was 2.42%. This was obtained
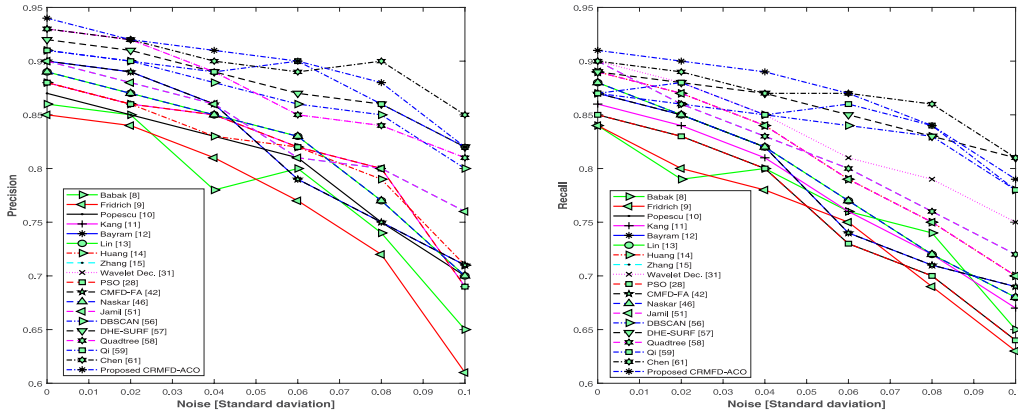
FIGURE 8. Comparison between existing algorithms and the proposed algorithm, while using Gaussian noise in view of DB-1.
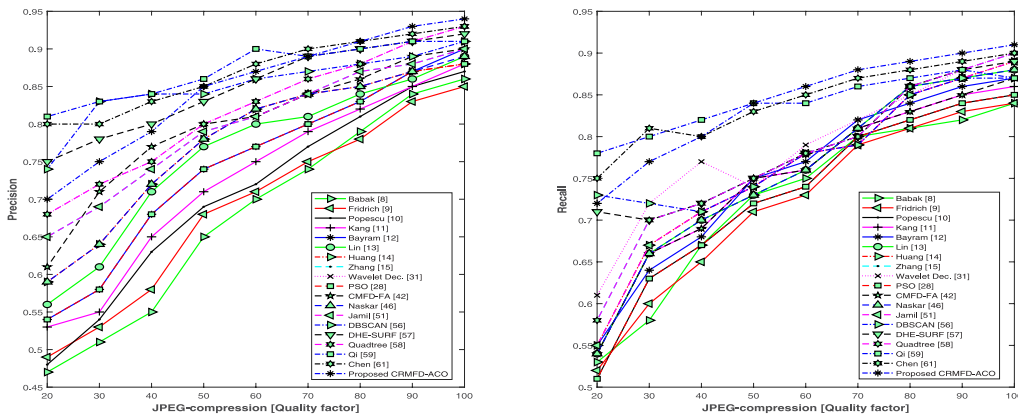

FIGURE 9. Comparison between existing algorithms and the proposed algorithm, while performing JPEG compression in view of DB-1.
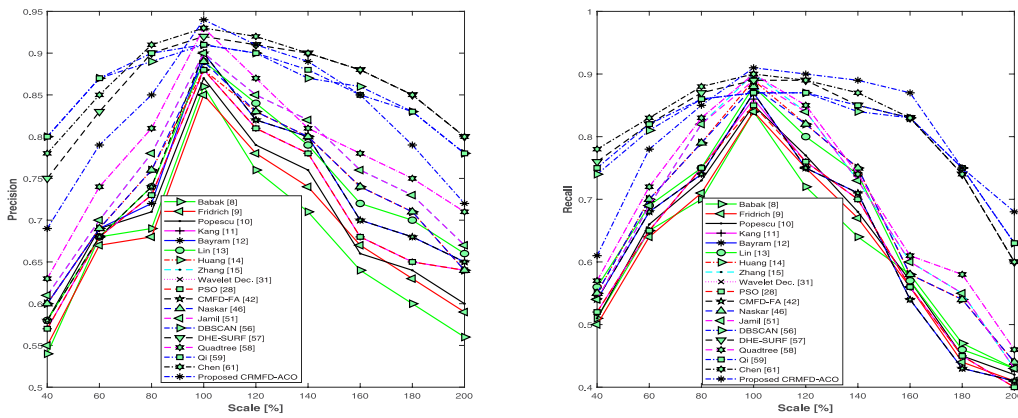

FIGURE 10. Comparison between existing algorithms and the proposed algorithm, while performing scaling in view of DB-1.

after a blind experiment was conducted by using a mixture of tempered and real images from the dataset. Compared to the current methods, it was determined that the proposed algorithm achieved higher improvements in the F1-score, recall, and precision, from 0.56% to 12.81%, 0.31% to 13.67%, and 0.84% to 13.01%, respectively.

MICC-F2000 (DB-3) consists of 2000 photographs, of which 700 are fake and 1300 are real. Considering DB-3, Fig. 7 shows several instances of real photographs, fake photographs, and their detection results. According to Table 4, the F1-score, recall, and precision for the proposed and specific existing systems are specified in light of DB-3. The average
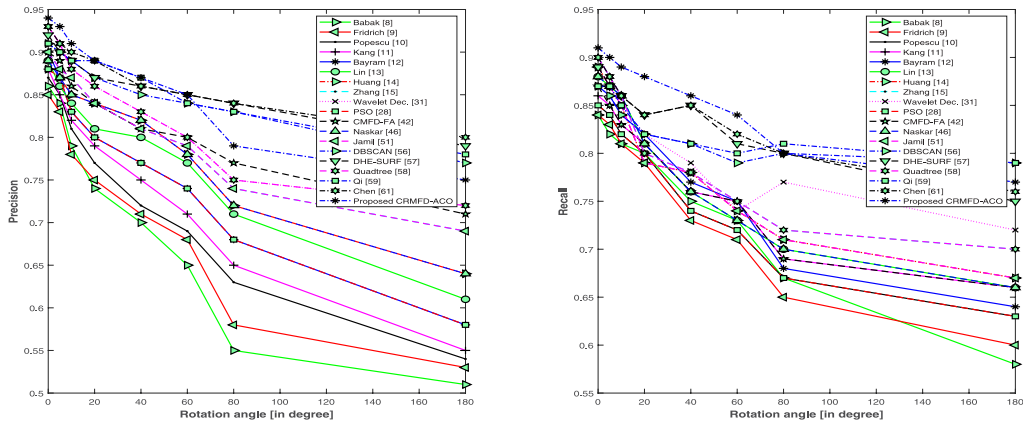
FIGURE 11. Comparison between existing algorithms and the proposed algorithm, while performing a rotation in view of DB-1.
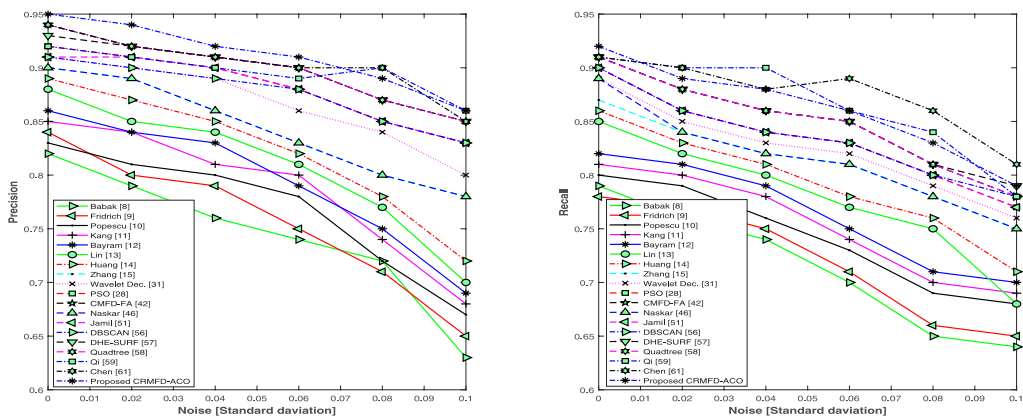

FIGURE 12. Comparison between existing algorithms and the proposed algorithm, while using Gaussian noise in view of DB-2.
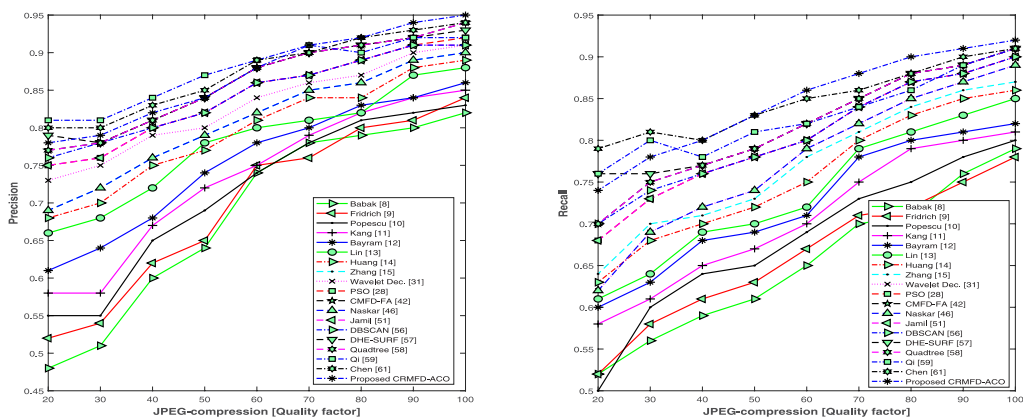

FIGURE 13. Comparison between existing algorithms and the proposed algorithm, while performing JPEG compression in view of DB-2.

F1-score, recall, and precision of our proposed strategy were 96.10%, 95.10%, and 97.14%, respectively, and the accuracy of the estimated recognition of ill-defined situations in doctored pictures was 1.18%. This result was obtained after a blind experiment was conducted using a mixture of tempered and real images in the dataset. Comparing the proposed approach to the current ones, greater improvements were achieved in the F1-score, recall, and precision from 0.77% to 9.89%, 0.66% to 9.26%, and 0.9% to 11.33%, respectively.
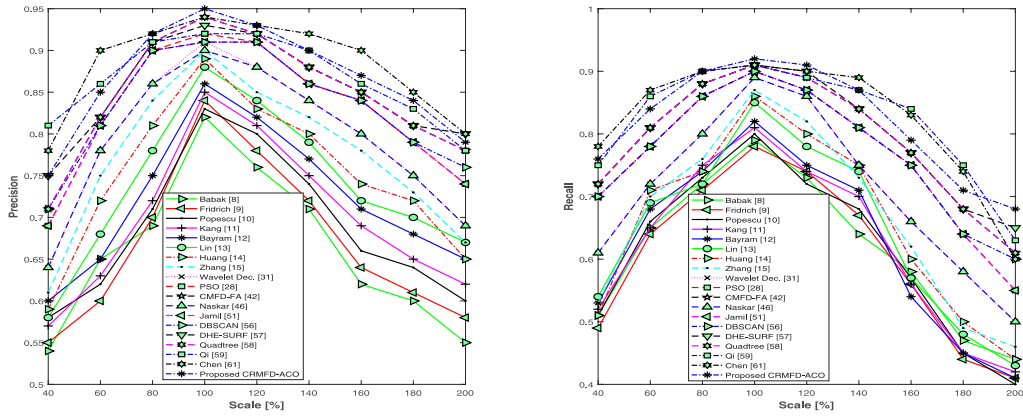
FIGURE 14. Comparison between existing algorithms and the proposed algorithm, while performing scaling in view of DB-2.
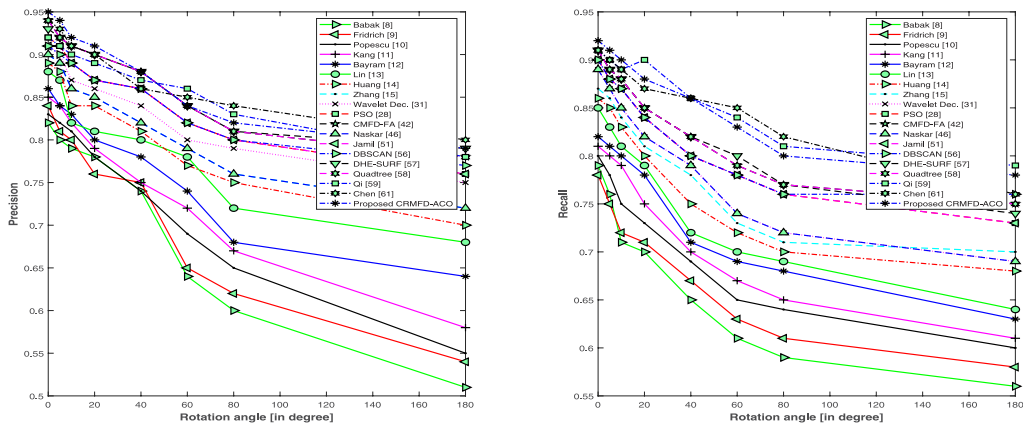

FIGURE 15. Comparison between existing algorithms and the proposed algorithm, while performing rotation in view of DB-2.
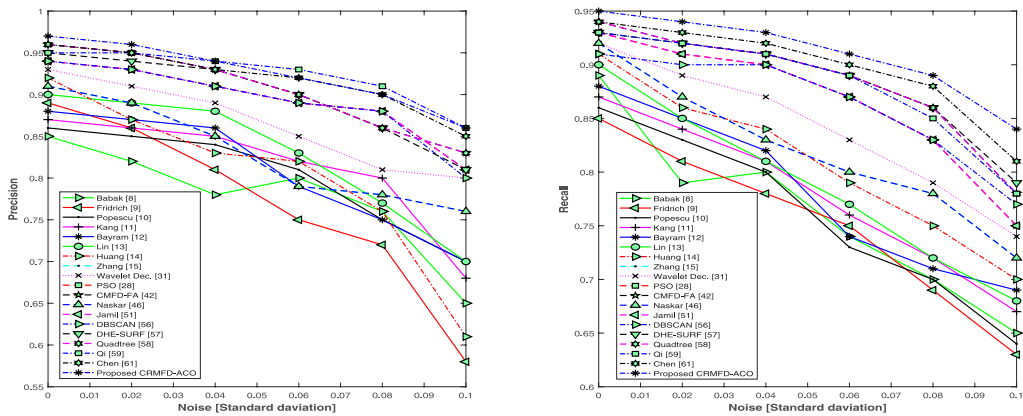

FIGURE 16. Comparison between existing algorithms and the proposed algorithm, while using Gaussian noise in view of DB-3.

Efficacy of the proposed CRMFD-ACO was tested in the presence of a variety of assaults, including straightforward copy-rotate-move phony, addition of Gaussian noise to the tempered region to hide its presence, JPEG compression, rotation, and scaling. Figures 8, 12, and 16 depict a comparison of the proposed algorithm with existing methods when noise or commotion is introduced to the tempered

region. As shown in Figures 8, 12, and 16, the recall and precision values were reduced by adding zero-mean Gaussian commotion with standard deviations of 0.02, 0.04, 0.06, 0.08, and 0.10.

Comparison between the current methods and the suggested technique is shown in Figures 9, 13 and 17, where JPEG compression was applied to the tempered region of the
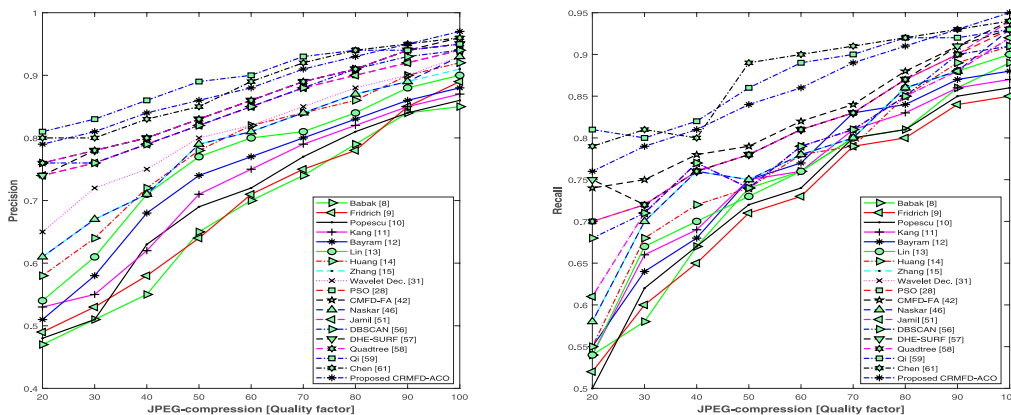
FIGURE 17. Comparison between existing algorithms and the proposed algorithm, while performing JPEG compression in view of DB-3.
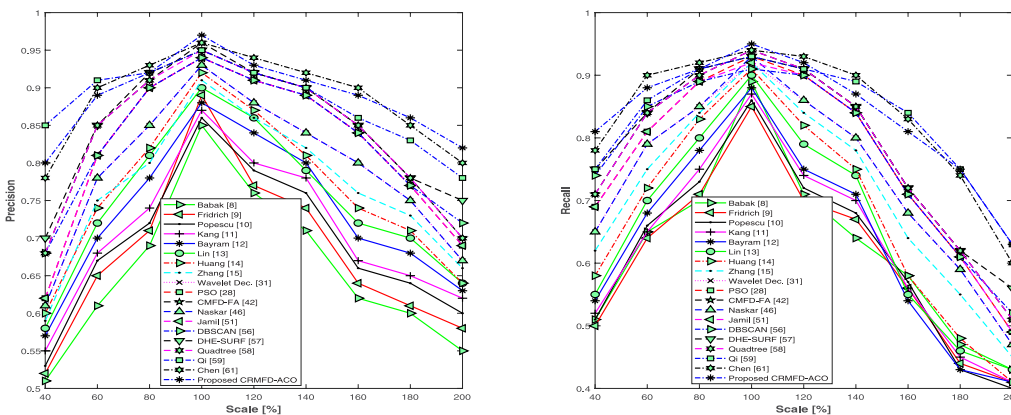

FIGURE 18. Comparison between existing algorithms and the proposed algorithm, while performing scaling in view of DB-3.
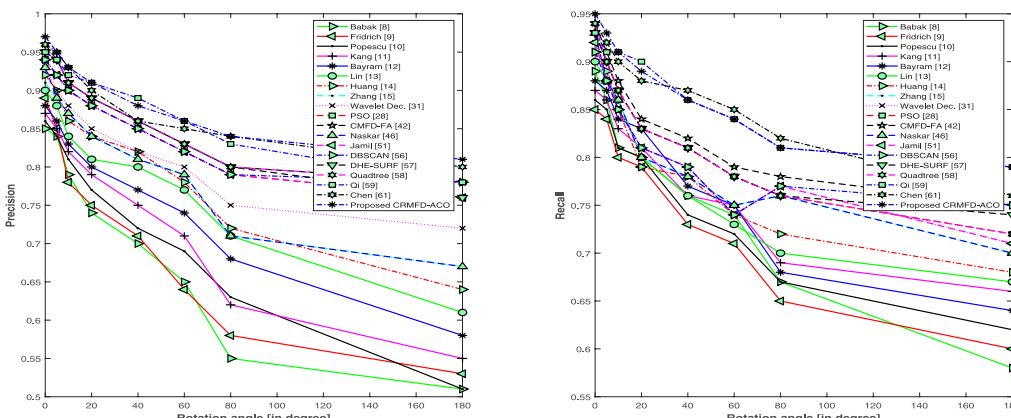
FIGURE 19. Comparison between existing algorithms and the proposed algorithm, while performing rotation in view of DB-3.

fabricated image to make it more subdued. The recall and precision values decreased with a change in JPEG-compression quality from 100 to 20 in the means of 10 degrees, as shown in Figures 9, 13, and 17. Figures 10, 14, and 18 show the comparisons between the existing and proposed algorithms.

When the scaling activity was performed in the tempered region, recall and precision achieved higher values. However, the tempered areas were not scaled in the proposed CRMFD-ACO algorithm. When the tempered regions were scaled back by factors of 40%, 60%, 80%,

TABLE 2. Performance evaluation of the proposed algorithm and existing algorithms for copy-rotate-move tempering in view of DB-1.

Methods	Precision (%)	Recall (%)	F1 (%)
Babak [8]	86.17	84.27	85.20940976
Fridrich [9]	85.2	84.29	84.74255708
Popescu [10]	87.19	85.19	86.17839773
Kang [11]	88.1	86.45	87.26720137
Bayram [12]	90.14	87.46	88.77977928
Lin [13]	89.67	88.26	88.95941325
Huang [14]	88.24	89.17	88.70256243
Zhang [15]	90.16	90.18	90.16999889
Wavelet Dec. [31]	93.89	90.16	91.98720348
PSO [28]	88.67	85.19	86.89517198
CMFD-FA [42]	90.25	87.45	88.82794035
Naskar [46]	88.26	88.15	88.2049657
Jamil [51]	90.11	89.28	89.69307988
DBSCAN [56]	91.67	87.51	89.5417089
DHE-SURF [57]	92.83	89.12	90.93717615
Quadtree [58]	93.59	90.1	91.81184604
Qi [59]	91.63	87.52	89.52785487
Chen [61]	93.19	90.78	91.96921455
CRMFD-ACO	94.44	91.89	93.14755112

TABLE 3. Performance evaluation of the proposed algorithm and existing algorithms for copy-rotate-move tempering in view of DB-2.

Methods	Precision (%)	Recall (%)	F1 (%)
Babak [8]	82.31	79.48	80.87024909
Fridrich [9]	84.07	78.42	81.14677088
Popescu [10]	83.37	80.3	81.80620761
Kang [11]	85.71	81.65	83.63075406
Bayram [12]	86.45	82.09	84.21360508
Lin [13]	88.37	85.31	86.81304353
Huang [14]	89.32	86.78	88.031682
Zhang [15]	90.42	87.73	89.05469099
Wavelet Dec. [31]	91.42	89.12	90.25534951
PSO [28]	92.51	90.34	91.4121236
CMFD-FA [42]	94.48	91.78	93.11043058
Naskar [46]	90.49	89.38	89.93157503
Jamil [51]	91.69	90.11	90.89313421
DBSCAN [56]	91.62	90.03	90.81804129
DHE-SURF [57]	93.17	91.39	92.27141634
Quadtree [58]	94.35	91.24	92.76894229
Qi [59]	92.56	91.07	91.80895496
Chen [61]	94.13	91.27	92.67794067
CRMFD-ACO	95.32	92.09	93.67716557

TABLE 4. Performance evaluation of the proposed algorithm and existing algorithms for copy-rotate-move tempering in view of DB-3.

Methods	Precision (%)	Recall (%)	F1 (%)
Babak [8]	85.81	89.37	87.55382692
Fridrich [9]	89.15	85.84	87.46369507
Popescu [10]	86.29	86.14	86.21493476
Kang [11]	87.17	87.34	87.2549172
Bayram [12]	88.25	88.42	88.33491821
Lin [13]	90.51	90.14	90.32462109
Huang [14]	92.49	91.37	91.92658871
Zhang [15]	91.39	92.12	91.75354804
Wavelet Dec. [31]	93.45	92.85	93.14903382
PSO [28]	94.37	93.82	94.09419629
CMFD-FA [42]	96.24	94.44	95.33150409
Naskar [46]	93.15	93.48	93.31470825
Jamil [51]	94.36	92.58	93.46152562
DBSCAN [56]	94.86	91.54	93.17043348
DHE-SURF [57]	95.35	93.71	94.52288691
Quadtree [58]	95.59	94.28	94.93048086
Qi [59]	95.62	93.26	94.42525625
Chen [61]	96.24	94.17	95.19374823
CRMFD-ACO	97.14	95.1	96.10917603

TABLE 5. Comparison of the computational performance between the existing algorithm and the proposed algorithm for copy-rotate-move forgery detection.

Methods	Processor Utilization	RAM Exigency	Execution and Validation Time in seconds
Bayram [12]	89 %	14.0 GB	239
Lin [13]	91 %	13.9 GB	245
Huang [14]	92 %	14.1 GB	250
Zhang [15]	91 %	14.7 GB	240
PSO [28]	88 %	14.6 GB	156
CMFD-FA [42]	90 %	15.3 GB	190
Naskar [46]	79 %	14.4 GB	210
Jamil [51]	82 %	13.9 GB	198
DBSCAN [56]	79 %	13.8 GB	168
DHE-SURF [57]	75 %	12.2 GB	145
Quadtree [58]	85 %	14.8 GB	205
Qi [59]	58 %	10.2 GB	82
Chen [61]	55 %	10.5 GB	85
CRMFD-ACO	52 %	9.8 GB	80

120%, 140%, 160%, 160%, and 200%, their characteristics were reduced to lower values, and recall and precision values decreased. Moreover, the tempered area was rotated between 5 degrees and 20 degrees in strides of 5 degrees, which also reduced recall and precision values. Figures 11, 15, and 19 show the comparison between the existing algorithms and the proposed algorithm when rotation is performed on the tempered area. Table 2 shows the performance evaluation of the proposed and existing algorithms for copy-rotate-move tempering in view of DB-1. The proposed CRMFD-ACO algorithm achieved higher precision, recall, and F1-score values compared to other existing algorithms. The total average time required for the execution of the proposed algorithm is 80 seconds, which is faster because of the lower computational complexity of the proposed algorithm than other conventional models such as Bayram et al. [12], Lin et al. [13], Huang et al. [14], Zhang et al. [15], PSO [28], CMFD-FA [42], Dixit and Naskar [46], Ahmed et al. [51], DBSCAN [56], DHE-SURF [57], Quadtree [58], Qi et al. [59], and Chen et al. [61], as summarized in Table 5.

V. CONCLUSION

This study provides a new, computationally strong approach for recognizing the fashioned portion of a modified image, created by a knowledgeable forger. The proposed algorithm subsequently generated modified parameter values, identified the fabricated area in the tested image, and demonstrated a high ability to detect copy-rotate-move phony in the processed image, even in the presence of JPEG compression, scaling, contrast change, blur, noise, and rotation. The proposed algorithm was tested on the MICC-F220 (DB-1), MICC-F600 (DB-2), and MICC-F2000 (DB-3) datasets. It had an average F1-score, recall, and precision of 93.15%, 91.89%, and 94.44%, respectively, for DB-1. Similarly, obtaining the F1 score, recall, and precision for the other two datasets is very promising. It was determined that the proposed algorithm achieved higher improvements in the F1-score, recall, and precision from 1.16% to 8.41%, 1.01% to 7.62%, and 0.55% to 8.27%, respectively, compared to the baseline. The proposed method is also compared with other state-of-the-art techniques, and the results demonstrate that it outperforms the existing methods. The proposed method is applicable only to copy-move forgery. If other types of

forgery, such as splicing and image re-sampling, are present in the processed image and other irregularities that are not apparent, researchers may develop advanced algorithms to detect a wide variety of image tempering.

REFERENCES

[1] H. Farid, "Image forgery detection," *IEEE Signal Process. Mag.*, vol. 26, no. 2, pp. 16–25, Mar. 2009.

[2] A. Phan-Ho and F. Retraint, "A comparative study of Bayesian and Dempster–Shafer fusion on image forgery detection," *IEEE Access*, vol. 10, pp. 99268–99281, 2022, doi: 10.1109/ACCESS.2022.3206543.

[3] K. M. Hosny, A. M. Mortda, M. M. Fouda, and N. A. Lashin, "An efficient CNN model to detect copy-move image forgery," *IEEE Access*, vol. 10, pp. 48622–48632, 2022, doi: 10.1109/ACCESS.2022.3172273.

[4] S. I. Lee, J. Y. Park, and I. K. Eom, "CNN-based copy-move forgery detection using rotation-invariant wavelet feature," *IEEE Access*, vol. 10, pp. 106217–106229, 2022, doi: 10.1109/ACCESS.2022.3212069.

[5] Y. Zhang, G. Zhu, X. Wang, X. Luo, Y. Zhou, H. Zhang, and L. Wu, "CNN-transformer based generative adversarial network for copy-move source/target distinguishment," *IEEE Trans. Circuits Syst. Video Technol.*, vol. 33, no. 5, pp. 2019–2032, May 2023, doi: 10.1109/TCSVT.2022.3220630.

[6] A. Gu, J. Nam, and S. Lee, "FBI-Net: Frequency-based image forgery localization via multitask learning with self-attention," *IEEE Access*, vol. 10, pp. 62751–62762, 2022, doi: 10.1109/ACCESS.2022.3182024.

[7] M. Kaya, K. J. Sani, and S. Karakus, "Copy-move forgery detection in digital forensic images using CNN," in *Proc. 7th Int. Conf. Comput. Sci. Eng. (UBMK)*, Sep. 2022, pp. 239–245, doi: 10.1109/UBMK55850.2022.9919560.

[8] B. Mahdian and S. Saic, "Detection of copy–move forgery using a method based on blur moment invariants," *Forensic Sci. Int.*, vol. 171, nos. 2–3, pp. 180–189, Sep. 2007.

[9] J. Fridrich, D. Soukal, and J. Lukas, "Detection of copy-move forgery in digital images," in *Proc. Digit. Forensic Res. Workshop (DFRWS)*, Cleveland, OH, USA, Sep. 2003, pp. 134–137.

[10] A. C. Popescu and H. Farid, "Exposing digital forgeries by detecting duplicated image regions," Dept. Comput. Sci., Dartmouth College, Hanover, NH, USA, Tech. Rep. TR2004-515, 2004.

[11] X. Kang and S. Wei, "Identifying tampered regions using singular value decomposition in digital image forensics," in *Proc. Int. Conf. Comput. Sci. Softw. Eng.*, 2008, pp. 926–930.

[12] S. Bayram, H. Taha Sencar, and N. Memon, "An efficient and robust method for detecting copy-move forgery," in *Proc. IEEE Int. Conf. Acoust., Speech Signal Process.*, Apr. 2009, pp. 1053–1056.

[13] H. J. Lin, C. W. Wang, and Y. T. Kao, "Fast copy-move forgery detection," *WSEAS Trans. Signal Process.*, vol. 5, no. 5, pp. 188–197, 2009.

[14] Y. Huang, W. Lu, W. Sun, and D. Long, "Improved DCT-based detection of copy-move forgery in images," *Forensic Sci. Int.*, vol. 206, nos. 1–3, pp. 178–184, Mar. 2011.

[15] H. Shabanian and F. Mashhadi, "A new approach for detecting copy-move forgery in digital images," in *Proc. IEEE Western New York Image Signal Process. Workshop (WNYISPW)*, Nov. 2017, pp. 1–6.

[16] M. Dorigo, "Optimization, learning and natural algorithms," Ph.D. thesis, Dept. Electron., Polytech. Milan, Milan, Italy, 1992, pp. 134–142.

[17] M. Dorigo and T. Stutzle, *Ant Colony Optimization*. Cambridge, MA, USA: MIT Press, 2004.

[18] X. S. Yang, J. M. Lees, and C. T. Morley, "Application of virtual ant algorithms in the optimization of CFRP shear strengthened precracked structures," in *Proc. Int. Conf. Comput. Sci.*, vol. 3991, 2006, pp. 834–837.

[19] M.-K. Hu, "Visual pattern recognition by moment invariants," *IEEE Trans. Inf. Theory*, vol. IT-8, no. 2, pp. 179–187, Feb. 1962.

[20] H. Shin Kim and H.-K. Lee, "Invariant image watermark using Zernike moments," *IEEE Trans. Circuits Syst. Video Technol.*, vol. 13, no. 8, pp. 766–775, Aug. 2003.

[21] C.-H. Teh and R. T. Chin, "On image analysis by the methods of moments," *IEEE Trans. Pattern Anal. Mach. Intell.*, vol. 10, no. 4, pp. 496–513, Jul. 1988.

[22] A. Khotanzad and Y. H. Hong, "Invariant image recognition by Zernike moments," *IEEE Trans. Pattern Anal. Mach. Intell.*, vol. 12, no. 5, pp. 489–497, May 1990.

[23] F. Zernike, "Beugungstheorie des Schneidenverfahrens und seiner verbesserten form, der phasenkontrastmethode," *Physica*, vol. 1, pp. 689–704, May 1934.

[24] J. Flusser and T. Suk, "Degraded image analysis: An invariant approach," *IEEE Trans. Pattern Anal. Mach. Intell.*, vol. 20, no. 6, pp. 590–603, Jun. 1998.

[25] J. Flusser, T. Suk, and S. Saic, "Recognition of blurred images by the method of moments," *IEEE Trans. Image Process.*, vol. 5, no. 3, pp. 533–538, Mar. 1996.

[26] J. Flusser, T. Suk, and S. Saic, "Image features invariant with respect to blur," *Pattern Recognit.*, vol. 28, no. 11, pp. 1723–1732, Nov. 1995.

[27] V. Christlein, C. Riess, J. Jordan, C. Riess, and E. Angelopoulou, "An evaluation of popular copy-move forgery detection approaches," *IEEE Trans. Inf. Forensics Security*, vol. 7, no. 6, pp. 1841–1854, Dec. 2012.

[28] S. Wenchang, Z. Fei, Q. Bo, and L. Bin, "Improving image copy-move forgery detection with particle swarm optimization techniques," *China Commun.*, vol. 13, no. 1, pp. 139–149, Jan. 2016.

[29] X. S. Yang, "Engineering optimization: An introduction with metaheuristic applications," in *Forensic Science International*. Hoboken, NJ, USA: Wiley, 2010.

[30] Q. Liu, A. H. Sung, M. Qiao, Z. Chen, and B. Ribeiro, "An improved approach to steganalysis of JPEG images," *Inf. Sci.*, vol. 180, no. 9, pp. 1643–1655, May 2010.

[31] A. Kashyap and S. D. Joshi, "Detection of copy-move forgery using wavelet decomposition," in *Proc. Int. Conf. SIGNAL Process. Commun. (ICSC)*, Dec. 2013, pp. 396–400.

[32] A. C. Popescu and H. Farid, "Exposing digital forgeries by detecting traces of resampling," *IEEE Trans. Signal Process.*, vol. 53, no. 2, pp. 758–767, Feb. 2005.

[33] H. Farid, "Creating and detecting doctored and virtual images: Implications to the child pornography prevention act," Dartmouth College, Hanover, NH, USA, Tech. Rep. 2004-518, 2004.

[34] J. Fridrich, D. Soukal, and J. Lukas, "Detection of copy move forgery in digital images," *Int. J. Comput. Sci.*, vol. 3, pp. 55–61, Jan. 2003.

[35] J. Shlens, *A Tutorial on Principal Component Analysis, Derivation, Discussion and Singular Value Decomposition, Version 1*, Mar. 2003.

[36] S. Khan and A. Kulkarni, "Robust method for detection of copy-move forgery in digital images," in *Proc. Int. Conf. Signal Image Process.*, Chennai, India, 2010, pp. 69–73, doi: 10.1109/ICSIP.2010.5697444.

[37] T. M. Shami, A. A. El-Saleh, M. Alswaitti, Q. Al-Tashi, M. A. Summakieh, and S. Mirjalili, "Particle swarm optimization: A comprehensive survey," *IEEE Access*, vol. 10, pp. 10031–10061, 2022, doi: 10.1109/ACCESS.2022.3142859.

[38] N. Lopac, I. Jurdana, J. Lerga, and N. Wakabayashi, "Particle-swarm-optimization-enhanced radial-basis-function-kernel-based adaptive filtering applied to maritime data," *J. Mar. Sci. Eng.*, vol. 9, no. 4, p. 439, Apr. 2021, doi: 10.3390/jmse9040439.

[39] M. Barni, A. Costanzo, and L. Sabatini, "Identification of cut & paste tampering by means of double-JPEG detection and image segmentation," in *Proc. IEEE Int. Symp. Circuits Syst.*, May 2010, pp. 1687–1690.

[40] Z. Zhang, Z. Yu, and B. Su, "Detection of composite forged image," in *Proc. Int. Conf. Comput. Appl. Syst. Model. (ICCASM)*, vol. 11, Oct. 2010, pp. V11-572–V11-576.

[41] J. He, Z. Lin, L. Wang, and X. Tang, "Detecting doctored JPEG images via DCT coefficient analysis," in *Computer Vision ECCV 2006* (Lecture Notes in Computer Science), vol. 3953. Berlin, Germany: Springer, 2006, pp. 423–435.

[42] A. Kashyap, B. Suresh, and H. Gupta, "Robust detection of copy-move forgery based on wavelet decomposition and firefly algorithm," *Comput. J.*, vol. 65, no. 4, pp. 983–996, Apr. 2022.

[43] W. Li, Y. Yuan, and N. Yu, "Detecting copy-paste forgery of jpeg image via block artifact grid extraction," in *Proc. Int. Workshop Local Non-Local Approximation Image Process.*, 2008, pp. 1–6.

[44] E. Ardizzone, A. Bruno, and G. Mazzola, "Copy-move forgery detection via texture description," in *Proc. 2nd ACM Workshop Multimedia Forensics, Secur. Intell.*, Oct. 2010, pp. 59–64.

[45] S. Teerakanok and T. Uehara, "Copy-move forgery detection: A state-of-the-art technical review and analysis," *IEEE Access*, vol. 7, pp. 40550–40568, 2019.

[46] R. Dixit and R. Naskar, "Copy-rotate-move forgery detection using complex wavelet transform and local binary pattern," in *Proc. 10th Int. Conf. Comput., Commun. Netw. Technol. (ICCCNT)*, Jul. 2019, pp. 1–7.

[47] Y. Li, J. Zhou, A. Cheng, X. Liu, and Y. Y. Tang, "SIFT keypoint removal and injection via convex relaxation," *IEEE Trans. Inf. Forensics Security*, vol. 11, no. 8, pp. 1722–1735, Aug. 2016.

[48] O. Mayer and M. C. Stamm, "Forensic similarity for digital images," *IEEE Trans. Inf. Forensics Security*, vol. 15, pp. 1331–1346, 2020.

[49] C. Yan and C. Pun, "Multi-scale difference map fusion for tamper localization using binary ranking hashing," *IEEE Trans. Inf. Forensics Security*, vol. 12, no. 9, pp. 2144–2158, Sep. 2017.

[50] Y. Liu, C. Xia, X. Zhu, and S. Xu, "Two-stage copy-move forgery detection with self deep matching and proposal SuperGlue," *IEEE Trans. Image Process.*, vol. 31, pp. 541–555, 2022.

[51] I. T. Ahmed, B. T. Hammad, and N. Jamil, "Image copy-move forgery detection algorithms based on spatial feature domain," in *Proc. IEEE 17th Int. Colloq. Signal Process. Appl. (CSPA)*, Mar. 2021, pp. 92–96.

[52] V. A. K. Raj, "Digital image tamper detection tools," M.S. thesis, Forschungszentrum Karlsruhe, Karlsruhe Univ. Appl. Sci., Karlsruhe, Germany, 2005.

[53] I. Daubechies, *Ten Lectures on Wavelets*. Philadelphia, PA, USA: Society for Industrial and Applied Mathematics, 1992.

[54] I. Daubechies, "Orthonormal bases of compactly supported wavelets," *Commun. Pure Appl. Math.*, vol. 41, no. 7, pp. 909–996, Oct. 1988.

[55] R. John Williams and K. Amaratungay, "Introduction to wavelets in engineering,," *Int. J. Numer. Methods Eng.*, vol. 37, no. 14, pp. 2365–2388, 1994.

[56] M. Bilal, H. A. Habib, Z. Mehmood, T. Saba, and M. Rashid, "Single and multiple copy–move forgery detection and localization in digital images based on the sparsely encoded distinctive features and DBSCAN clustering," *Arabian J. Sci. Eng.*, vol. 45, no. 4, pp. 2975–2992, Apr. 2020.

[57] M. Bilal, H. A. Habib, Z. Mehmood, R. M. Yousaf, T. Saba, and A. Rehman, "A robust technique for copy-move forgery detection from small and extremely smooth tampered regions based on the DHE-SURF features and mDBSCAN clustering," *Austral. J. Forensic Sci.*, vol. 53, no. 4, pp. 1–24, 2021, doi: 10.1080/00450618.2020.1715479.

[58] G. Muzaffer, G. Ulutas, and B. Ustubioglu, "Copy move forgery detection with quadtree decomposition segmentation," in *Proc. 43rd Int. Conf. Telecommun. Signal Process. (TSP)*, Jul. 2020, pp. 208–211.

[59] S. Qi, Y. Zhang, C. Wang, J. Zhou, and X. Cao, "A principled design of image representation: Towards forensic tasks," *IEEE Trans. Pattern Anal. Mach. Intell.*, vol. 45, no. 5, pp. 5337–5354, May 2023, doi: 10.1109/TPAMI.2022.3204971.

[60] C. R. Gonzalez, E. R. Woods, and L. S. Eddins, *Digital Image Processing Using MATLAB*. London, U.K.: Pearson, 2003.

[61] B. Chen, W. Tan, G. Coatrieux, Y. Zheng, and Y. Shi, "A serial image copy-move forgery localization scheme with source/target distinguishment," *IEEE Trans. Multimedia*, vol. 23, pp. 3506–3517, 2021, doi: 10.1109/TMM.2020.3026868.

[62] I. Amerini, L. Ballan, R. Caldelli, A. Del Bimbo, and G. Serra, "A SIFT-based forensic method for copy–move attack detection and transformation recovery," *IEEE Trans. Inf. Forensics Security*, vol. 6, no. 3, pp. 1099–1110, Sep. 2011.

[63] H. S. Radeaf, B. M. Mahmmod, S. H. Abdulhussain, and D. Al-Jumaeily, "A steganography based on orthogonal moments," in *Proc. Int. Conf. Inf. Commun. Technol.*, Apr. 2019, pp. 147–153, doi: 10.1145/3321289.3321324.

[64] S. H. Abdulhussain, A. R. Ramli, A. J. Hussain, B. M. Mahmmod, and W. A. Jassim, "Orthogonal polynomial embedded image kernel," in *Proc. Int. Conf. Inf. Commun. Technol.*, Apr. 2019, pp. 215–221, doi: 10.1145/3321289.3321310.

[65] B. M. Mahmmod, S. H. Abdulhussain, T. Suk, and A. Hussain, "Fast computation of Hahn polynomials for high order moments," *IEEE Access*, vol. 10, pp. 48719–48732, 2022, doi: 10.1109/ACCESS.2022.3170893.

[66] Z. N. Idan, S. H. Abdulhussain, B. M. Mahmmod, K. A. Al-Utaibi, S. A. R. Al-Hadad, and S. M. Sait, "Fast shot boundary detection based on separable moments and support vector machine," *IEEE Access*, vol. 9, pp. 106412–106427, 2021, doi: 10.1109/ACCESS.2021.3100139.

[67] L. K. Jiwani, S. D. Joshi, and G. S. Visweswaran, "Spectral density driven wavelet representation of 2-D images," in *Proc. IEEE Int. Symp. Signal Process. Inf. Technol.*, Aug. 2006, pp. 138–143.

ABHISHEK KASHYAP received the B.Tech. degree in electronics and communication engineering from Uttar Pradesh Technical University, Lucknow, India, in 2009, and the M.Tech. and Ph.D. degrees from IIT Delhi, New Delhi, India, in 2013 and 2018, respectively. From 2009 to 2011, he was a Lecturer with Uttar Pradesh Technical University. He is currently an Assistant Professor with the Jaypee Institute of Information Technology, Noida, India. His research interests include signal processing and image processing using deep learning.

KAPIL DEV TYAGI received the B.E. degree in electronics and communication engineering from the University of Rajasthan, Jaipur, India, in 2003, the M.Tech. degree from IIT Delhi, New Delhi, India, in 2010, and the Ph.D. degree from CARE, IIT Delhi, in 2016. From 2003 to 2007, he was a Lecturer with Uttar Pradesh Technical University, Lucknow, India. From 2007 to 2008, he was a Scientist-C with Indian Space Research Organization, Bengaluru, India. He is currently an Assistant Professor with the Jaypee Institute of Information Technology, Noida, India. Since August 2016, he has done eight consultancy projects for CARE, IIT Delhi.

VAIBHAV BHUSHAN TYAGI received the B.Tech. degree from Uttar Pradesh Technical University, Lucknow, India, in 2007, and the M.Tech and Ph.D. degrees from IIT Roorkee, in 2011 and 2015, respectively. He is currently an Associate Professor (ECE) and the Dean FICT with ISBAT University, Kampala, Uganda. He is having more than 13 years of research and teaching experience around the globe. He was involved in several administrative and academic positions in India, Ethiopia, and Uganda. His research interests include sensor applications in signal processing, signal modeling, artificial intelligence, and deep learning.

• • •